

# X-ray flares, plateaus, and chromatic breaks of GRB afterglows from up-scattered forward-shock emission

A. Panaitescu

Space Science and Applications, MS D466, Los Alamos National Laboratory, Los Alamos, NM 87545, USA

## ABSTRACT

Scattering of the forward-shock synchrotron emission by a relativistic outflow located behind the leading blast-wave may produce an X-ray emission brighter than that coming directly from the forward-shock and may explain four features displayed by Swift X-ray afterglows: flares, plateaus (slow decays), chromatic light-curve breaks, and fast post-plateau decays. For a cold scattering outflow, the reflected flux overshines the primary one if the scattering outflow is nearly baryon-free and highly relativistic. These two requirements can be relaxed if the scattering outflow is energized by weak internal shocks, so that the incident forward-shock photons are also inverse-Compton scattered, in addition to bulk-scattering. Sweeping-up of the photons left behind by the forward shock naturally yields short X-ray flares. Owing to the boost in photon energy produced by bulk-scattering scattering, the reflected emission is more likely to overshine that coming directly from the forward shock at higher photon energies, yielding light-curve plateaus and breaks that appear only in the X-ray. The brightness, shape, and decay of the X-ray light-curve plateau depend on the radial distribution of the scatterer’s Lorentz factor and mass-flux. Chromatic X-ray light-curve breaks and sharp post-plateau decays cannot be accommodated by the direct forward-shock emission and argue in favour of the scattering-outflow model proposed here. On the other hand, the X-ray afterglows without plateaus, those with achromatic breaks, and those with very long-lived power-law decays are more naturally accommodated by the standard forward-shock model. Thus the diversity of X-ray light-curves arises from the interplay of the scattered and direct forward-shock emissions.

**Key words:** radiation mechanisms: non-thermal - shock waves - gamma-rays: bursts

## 1 INTRODUCTION

A large fraction of X-ray afterglows of Gamma-Ray Bursts (GRBs) monitored by Swift in the last 2.5 years exhibit (Figure 1) *flares* (short, brightening episodes during which the X-ray flux increases by a factor up to 1000) and *plateaus* (power-law flux decays slower than expected in the standard blast-wave model, for the measured slope of the X-ray spectrum).

The short duration  $\delta t_{fwhm}$  of X-ray flares (Burrows et al 2007), half of which have  $\delta t_{fwhm}/t \lesssim 0.1$  (Chincarini et al 2007), is incompatible with an origin in the shock driven into the circumburst medium by the GRB ejecta (the *forward shock*) because its emission fluctuations cannot be both very bright and short-lived. If the fluctuation’s angular scale is  $\delta\theta \gtrsim \theta_{vis} \simeq \gamma^{-1}$ , with  $\gamma$  being the shock’s Lorentz factor (i.e. larger than the area visible to the observer), then the flare should last for  $\delta t \gtrsim \text{few} \times t$ , which is the spread in the photon arrival-time caused by the curvature of the visible emitting surface. If the fluctuation’s angular scale is less than  $\theta_{vis}$  ( $\delta\theta = \gamma^{-1}/n$ ,  $n > 1$ ), then the flare’s duration,  $\delta t \sim \text{few} \times t/n$ , can be arbitrarily small but the fluctuation’s surface brightness would have to be  $(1 - 10^3)n^2$  larger than that of the forward shock to overshine it and yield a flare

that is 1–1000 times brighter than the underlying forward-shock flux.

The inability of the forward shock to produce short and bright flares has been taken as indication (e.g. Zhang et al 2006) that flares originate from the same mechanism as the burst: internal shocks in a fluctuating outflow (Rees & Mészáros 1994). This model requires that the central engine producing the GRB ejecta must live for a lab-frame duration comparable to the observer time when the flare is seen.

The X-ray light-curve plateaus are generally smooth, thus a forward-shock interpretation is plausible. That, during the plateau, the X-ray flux decays slower than expected in the standard forward-shock model (e.g. Paczyński & Rhoads 1993, Mészáros & Rees 1997; Sari, Piran & Narayan 1998) requires that at least one of the assumptions of this model is invalid. As the X-ray flux depends on the blast-wave energy and the electron & magnetic field parameters in the forward shock, non-constancy of any of these quantities may explain the slow decay of X-ray plateaus: Nousek et al (2006), Panaitescu et al (2006a), and Zhang et al (2006) have proposed that energy is injected into the forward shock, Ioka et al (2006) studied the light-curves arising from evol-

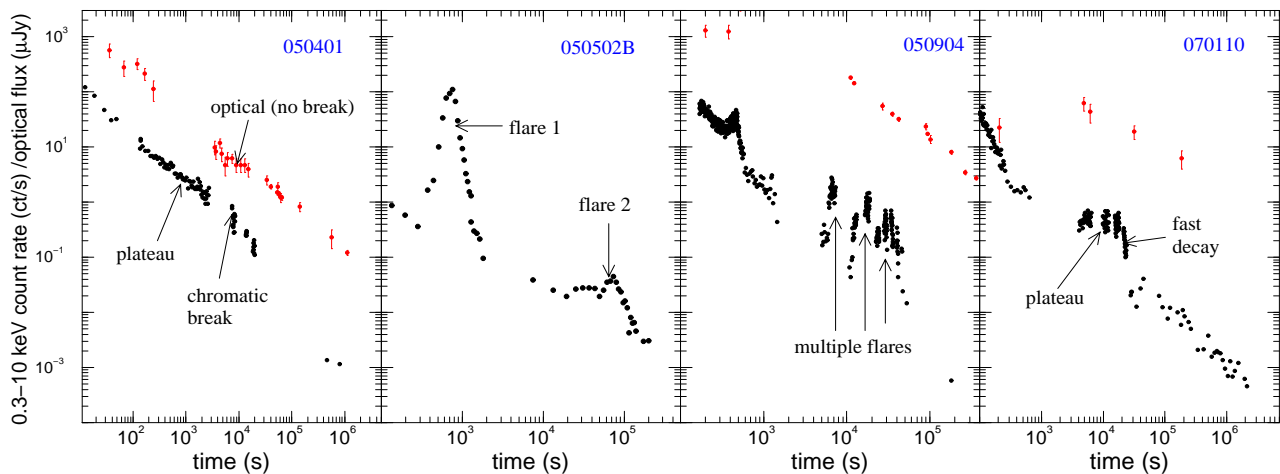


**Figure 1.** Examples of Swift afterglows exhibiting the following X-ray features: flares (GRB 050502B, 050904), plateaus (GRB 050401, 070110), fast post-plateau decay (GRB 070110), chromatic breaks (GRB 050401, 070110). Lower curves are the X-ray count rate (dots), upper curves are for the optical flux (red dots with error bars).

ing microphysical parameters, and Fan & Piran (2006) analyzed the afterglow emission when all three quantities evolve.

However, the existence of *chromatic* X-ray breaks at the end of some plateaus (e.g. GRB afterglows 050401 and 070110 shown in Figure 1), which are not exhibited by the optical light-curve, poses a serious problem to the above interpretation of plateaus because such a decoupling of the optical and X-ray emissions requires a strong spectral break to cross the X-ray range at the time of the chromatic break, yet the slope of the X-ray continuum is not observed to change across the break (Nousek et al 2006, Willingale et al 2007, Liang et al 2007).

The chromatic X-ray breaks may indicate that the afterglow emission arises from the reverse-shock crossing some inflowing, late ejecta that catch-up with the forward shock during the plateau. Again, to obtain the required decoupling of the optical and X-ray light-curves, a spectral break must be in between those domain: Uhm & Beloborodov (2007) attributed that break to the cooling of reverse-shock electrons, while Genet, Daigne & Mochkovitch (2007) identified it with the characteristic synchrotron frequency at which electrons would radiate if only 1 percent of reverse-shock electrons acquired equipartition energies. It remains to be investigated if, by tracking the cooling of forward-shock electrons during energy injection or by assuming that only 1 percent of them reach equipartition, the forward-shock acquires the same ability to decouple the optical and X-ray light-curves as the reverse shock may have.

In this paper, we continue to focus on the forward-shock emission, which naturally explains the power-law decay of afterglow light-curves, and investigate the possibility that the decoupling of the optical and X-ray emissions is due to a substantial contribution to the X-ray flux from an incoming, delayed outflow which up-scatters the forward-shock emission. Half of the synchrotron photons emitted by the forward shock are left behind it (the half which, in the shock frame, are emitted at an angle  $\alpha' > \pi/2$  relative to the radial direction of motion) and boosted relativistically by a factor ranging from  $\gamma$  (for  $\alpha' = \pi/2$ ) to  $(2\gamma)^{-1}$  (for  $\alpha' = \pi$ ).

The former are caught-up with by the incoming outflow if its Lorentz factor  $\Gamma$  is larger than that of the forward-shock; the latter will always be reached by the scattering outflow; for either, the Doppler boost after scattering is a factor  $(\Gamma/\gamma)^2$  higher than that of a forward-shock photon travelling directly toward the observer (i.e. the primary emission)

There are two reasons for which the up-scattered emission may be brighter than the primary. One is that the photon travel from place of emission to that of scattering delays the scattered emission relative to the direct forward-shock emission. Given that the latter decays, it follows that the scattered flux arriving at some time may be brighter than the forward-shock flux at same time. The second reason is at work if  $\Gamma > \gamma$ . In this case, scattering increases the photon energy more than the Doppler boost of the forward-shock does, so that, if the energy of the seed photon is above the peak of the synchrotron spectrum of the forward-shock emission, then the scattered flux at some observer-frame photon energy may exceed that of the forward-shock at same photon energy.

There is also one reason for which the scattered emission could be dimmer than the forward-shock's: for plausible kinetic energies of the scattering outflow (below about  $10^{53}$  erg) and the range of radii over which the up-scattering takes place (the forward-shock radius is  $10^{16} - 10^{17.5}$  cm), the scattering outflow is optically thin, thus only a small fraction of the photons left behind by the forward shock will be swept-up.

We assume that the scattering electrons are cold (i.e., in the frame of the incoming outflow, the primary photons do not gain energy through electron scattering). In this case, for the optical depth to electron scattering to be sufficiently large to yield a scattered flux brighter (at higher photon energies) than the forward-shock's, the scattering fluid must consist mostly of electron-positron pairs (i.e. baryon-poor), to maximize the number of leptons for a given kinetic energy and Lorentz factor of the scattering outflow.

Such a pair-enriched outflow are not expected from radiation-dominated fireballs, owing to pair-annihilation

above the photospheric radius, but could result in electromagnetic (Poynting) outflows (Lyutikov 2006) from the dissipation of magnetic around the deceleration radius. The latter model has received support from the timing of fast-decaying GRB tails and the epoch when the forward-shock emission emerges, which suggest that the burst and early afterglow emissions are produced at comparable radii ( $10^{15-16}$  cm, Kumar et al 2007). This is a plausible feature of the electromagnetic model and disfavours the internal-shock model for GRBs for which the subsecond burst variability timescale requires the GRB emission to be produced at  $10^{13-14}$  cm. Alternatively, if the short burst variability can be produced at larger radii, then the proximity of the locations where the burst and early afterglow emissions are released would point to internal-external shocks occurring between some incoming ejecta and the decelerating forward-shock (Fenimore & Ramirez-Ruiz 1999; Ramirez-Ruiz, Merloni & Rees 2001).

However, if the scattering electrons are hot (e.g. accelerated by internal shocks), then inverse-Compton scattering of forward-shock photons will boost into the X-rays seed photons of even lower energy, which may be numerous enough to compensate for the lower optical thickness of a scattering outflow with a normal baryon-to-lepton load. Thus, a hot outflow with a normal proton-to-electron composition (as expected for fireballs accelerated by radiation pressure) may still yield a scattered flux overshining in the X-rays that from the forward shock.

## 2 SET-UP

*Notations:* primed quantities are measured in the frame of the emitting fluid, unprimed are in the lab or observer frames; subscripts and superscripts "sc" and "fs" refer to scattering fluid and forward-shock quantities, respectively;  $\Gamma$  and  $R$  are the scatterer's Lorentz factor and radius,  $\gamma$  and  $r$  are those of the forward shock;  $t$  denotes lab-frame time,  $T$  is for observer (photon arrival) time.

A scattering, relativistic outflow with a significant radial spread can be approximated as a sequence of shells of zero radial thickness, thus we begin by calculating the emission from a scattering surface. Both the forward shock and scattered emissions are integrated over the equal arrival-time surface defined by  $T = t - r \cos \omega$  where  $\omega$  is the angle between the direction of motion of the radiating fluid element and the center of explosion – observer axis. For analytical calculations, one can ignore the spread in the photon arrival-time caused by the spherical curvature of the emitting surface and restrict attention to  $\omega = 0$  (i.e. assume that the fluid is moving directly toward the observer). The only important effect of the surface curvature which must be taken into account that is that, for a source of Lorentz factor  $g$ , the observer receives emission from a patch of angular opening  $\omega_{max} = g^{-1}$  centered on the center–observer axis, as the emission from angles  $\omega > g^{-1}$  is less boosted relativistically. This means that the specific flux is

$$F(\nu) \propto \omega_{max}^2 g^3 I'(\nu/g) \propto g I'(\nu/g) \quad (1)$$

where  $\omega_{max}^2$  gives the source solid angle and  $g^3 I'(\nu/g)$  is the intensity of the relativistically-beamed emission of comoving frame intensity  $I'$ .

In the frame of the scattering outflow, the intensity  $I'_{sc}$

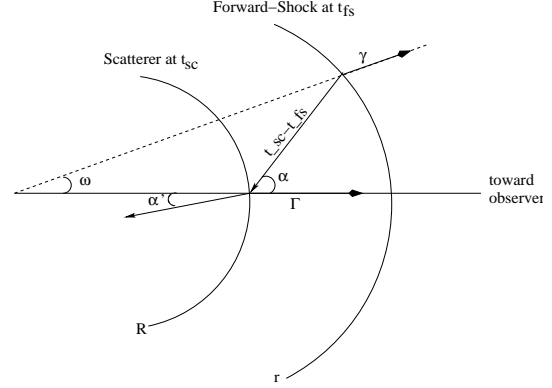


**Figure 2.** Geometry of scatterer and forward shock, moving at Lorentz factors  $\Gamma$  and  $\gamma$ , respectively. A forward-shock photon emitted at lab-frame time  $t_{fs}$  and moving at lab-frame angle  $\alpha$  (relative to the radially-out direction of flow) enters the scattering shell at time  $t_{sc}$  and scatterer-frame angle  $\alpha'$ .

of the radiation scattered in the radial direction is the integral over all incident angles  $\alpha'$  (see Figure 2) of the incoming radiation intensity  $I'_{in}$  times the electron cross-section for a photon deflection-angle  $\pi - \alpha'$  (i.e. the dipole pattern of electron scattering):

$$I'_{sc} = \frac{3}{8} \tau_{sc} \int_0^\pi d\alpha' \sin \alpha' (1 + \cos^2 \alpha') I'_{in}(\alpha') \quad (2)$$

where  $\tau_{sc} < 1$  is the optical thickness to electron-scattering of the scattering surface. For a scatterer of kinetic energy  $E_{sc} = 10^{53} E_{sc,53}$ , Lorentz factor  $\Gamma = 10^3 \Gamma_3$ , radius  $R = ct = 3 \times 10^{16} t_6$  cm, and  $N_e/N_p$  leptons per baryon

$$\tau_{sc} = 0.72 \times 10^{-2} \frac{E_{sc,53}}{\Gamma_3 t_6^2} \left( 1 + \frac{N_p m_p}{N_e m_e} \right)^{-1}. \quad (3)$$

If the curvature of the emitting surface is taken into account (as done numerically), the term  $1 + \cos^2 \alpha'$  of equation (2) is replaced by  $1 + \cos^2 \alpha' \cos^2 \omega' + \frac{1}{2} \sin^2 \alpha' \sin^2 \omega'$  where  $\omega'$  is the comoving-frame angle corresponding to the lab-frame  $\omega$ :  $\cos \omega' = (\cos \omega - B)/(1 - B \cos \omega)$ , with  $B = (1 - \Gamma^{-2})^{-1/2}$  being the *constant* velocity of the scattering surface.

The intensity  $I'_{in}(\alpha')$  of the incident radiation is the comoving intensity  $I'_{fs}$  of the forward-shock emission beamed relativistically by the relative motion of the scatterer and forward-shock. Considering specific intensities,

$$I'_{in}(\nu', \alpha') = D^3(\alpha) I'_{fs}(\nu'/D, \alpha) \quad (4)$$

where

$$D(\alpha) = \frac{\Gamma(1 + B \cos \alpha)}{\gamma[1 + b \cos(\alpha - \omega)]} \quad (5)$$

is the Doppler boost of the scatterer–forward-shock relative motion for a forward-shock photon moving at a lab-frame angle  $\pi - \alpha$  relative to the scatterer direction of motion, thus

$$\cos \alpha = \frac{\cos \alpha' - B}{1 - B \cos \alpha'}. \quad (6)$$

$b$  is the forward-shock velocity at the retarded time  $t_{fs}(t_{sc}, \alpha)$  when the photon arriving at scatterer at time  $t_{sc}$  and angle  $\alpha$  was emitted, and  $\omega(t_{fs}, \alpha)$  is the angle between the radial direction of motion of the forward-shock patch at angle  $\alpha$  and time  $t_{fs}$  and the direction toward the observer.

The kinematics of the photon motion from its place of emission  $(r, t_{fs})$  to that of scattering  $(R, t_{sc})$  provides two equations

$$r(t_{fs}) \cos \omega = R(t_{sc}) + (t_{sc} - t_{fs}) \cos \alpha \quad (7)$$

$$r(t_{fs}) \sin \omega = (t_{sc} - t_{fs}) \sin \alpha \quad (8)$$

from where the motion angle  $\omega$  and radius  $r(t_{fs})$  at the retarded time  $t_{fs}$  can be calculated. For the latter:

$$r^2 = R^2 + 2R(t_{sc} - t_{fs}) \cos \alpha + (t_{sc} - t_{fs})^2 \quad (9)$$

can be solved for  $t_{fs}$  using the equations for the scatterer's kinematics:

$$R(t_{sc}) = B(t_{sc} - t_{lag}) \simeq \left(1 - \frac{1}{2\Gamma^2}\right) (t_{sc} - t_{lag}) \quad (10)$$

where  $t_{lag}$  is the time elapsed between the ejection of the leading outflow producing the forward shock and the lagging scattering outflow, and for the forward-shock's motion:

$$r(t_{fs}) = \int_0^{t_{fs}} b(t) dt \simeq t_{fs} - \int_0^{t_{fs}} \frac{dt}{2\gamma^2(t)}. \quad (11)$$

The forward-shock dynamics resulting from sweeping-up and energizing a circumburst medium of particle density

$$n(r) \propto r^{-s} \quad (12)$$

is  $\gamma = \gamma_0$  until a "deceleration time"  $t_0$  when the reverse-shock crosses the relativistic ejecta, followed by

$$\gamma(t) = \gamma_0 \left(\frac{t}{t_0}\right)^{-(3-s)/2} \quad (s < 3). \quad (13)$$

Then, equation (11) yields

$$r(t_{fs}) \simeq t_{fs} \left[1 - \frac{1}{2(4-s)\gamma^2(t_{fs})}\right]. \quad (14)$$

Substituting equations (13) and (14) in (9) leads to the following equation for  $t_{fs}(t_{sc}, \alpha)$ :

$$2t_{fs} \left[ R \cos \alpha + t_{sc} - T_0 \left(\frac{t_{fs}}{t_0}\right)^{4-s} \right] = R^2 + 2Rt_{sc} \cos \alpha + t_{sc}^2 \quad (15)$$

where  $T_0 \equiv t_0/[2(4-s)\gamma_0^2]$  is the observer-frame deceleration time (i.e. the arrival-time of photons emitted by the forward-shock at the onset of its deceleration).

From equation (1), the flux received by the observer at time  $T_{sc}$  satisfies

$$F_{sc}(\nu, T_{sc}) \propto \Gamma I'_{sc}(\nu/\Gamma, t_{sc}) \quad (16)$$

where

$$T_{sc} = t_{sc} - R(t_{sc}) = t_{lag} + \frac{1}{2\Gamma^2}(t_{sc} - t_{lag}). \quad (17)$$

The flux received directly from the forward shock satisfies

$$F_{fs}(\nu, T_{fs}) \propto \gamma(t_{fs}) I'_{fs}(\nu/\gamma, t_{fs}) \quad (18)$$

with

$$T_{fs} = t_{fs} - r(t_{fs}) \simeq \frac{1}{2(4-s)} \frac{t_{fs}}{\gamma^2(t_{fs})} \quad (19)$$

which, together with equation (13), leads to

$$T_{fs} = T_0 \left(\frac{t_{fs}}{t_0}\right)^{4-s}, \quad \gamma(T_{fs}) = \gamma_0 \left(\frac{T_{fs}}{T_0}\right)^{-(3-s)/(8-2s)}. \quad (20)$$

It can be shown that, for times after the deceleration timescale  $T_0$ , the forward-shock Lorentz factor is

$$\gamma(T_{fs}) \simeq 450 \left(\frac{E_{fs,53}}{n_0}\right)^{1/8} T_{fs}^{-3/8} \quad (21)$$

for a homogeneous medium ( $s = 0$ ) and

$$\gamma(T_{fs}) \simeq 135 \left(\frac{E_{fs,53}}{A_*}\right)^{1/4} T_{fs}^{-1/4} \quad (22)$$

for a wind-like medium ( $s = 2$ ), with  $T_{fs}$  is measured in seconds,  $E_{fs,53}$  the forward-shock kinetic energy in  $10^{53}$  erg,  $n_0$  the circumburst medium density in protons/cm<sup>3</sup>,  $A_* = 1$  for the wind blown by a GRB progenitor with a mass-loss rate of  $dM_w/dt = 10^{-5} M_\odot \text{ yr}^{-1}$  and a terminal wind velocity of  $v = 1000 \text{ km s}^{-1}$ , and  $A_* \propto (dM_w/dt)/v$ .

Equations (2), (4), (16), and (18) relate the scattered flux with that received directly from the forward shock. To complete their numerical calculation, the comoving frame intensity  $I'_{fs}(\nu')$  of the forward-shock emission must be specified. For optically thin synchrotron, that intensity is

$$I'_{fs}(\nu') = I'_{fs}(\nu'_p) \begin{cases} (\nu'/\nu'_i)^{1/3} & \nu' < \nu'_i \\ (\nu'_i/\nu')^{(p-1)/2} & \nu'_i < \nu' < \nu'_c \\ (\nu'_c/\nu')^{1/2} & \nu'_c < \nu' < \nu'_i \\ (\nu'_i/\nu'_c)^{(p-1)/2} (\nu'_c/\nu)^{p/2} & \nu'_i, \nu'_c < \nu' \end{cases} \quad (23)$$

where  $p$  is the exponent of the power-law distribution of electrons with energy  $\epsilon$  in the forward shock –  $dn/d\epsilon \propto \epsilon^{-p}$  – and  $\nu'_i$  is the "injection" frequency (the characteristic synchrotron frequency at which the electrons of minimal energy radiate),  $\nu'_c$  is the "cooling" frequency (the characteristic frequency at which radiate the electrons whose radiative timescale equals the dynamical one), and  $I'_{fs}(\nu'_p)$  is the specific intensity at the peak  $\nu'_p = \min(\nu'_i, \nu'_c)$  of the forward-shock emission spectrum. Assuming that electrons and magnetic fields acquire constant fractions of the internal energy of the shocked medium, it can be shown that the spectral characteristics of the forward-shock emission have the following evolutions:

$$(t_{fs} < t_0) \quad I'_{fs}(\nu'_p) \propto t_{fs}^{3-1.5s}, \quad \nu'_i \propto t_{fs}^{-0.5s}, \quad \nu'_c \propto t_{fs}^{1.5s-2} \quad (24)$$

before deceleration and

$$(t_{fs} > t_0) \quad I'_{fs}(\nu'_p) \propto t_{fs}^{1.5-s}, \quad \nu'_i \propto t_{fs}^{s-4.5}, \quad \nu'_c \propto t_{fs}^{s-0.5} \quad (25)$$

after deceleration. In general, scattering of the pre-deceleration forward-shock emission yields a negligible contribution to the total scattered flux because, before deceleration, the forward-shock bolometric emission increases with time, thus the incident flux is largest at deceleration or after that.

### 3 X-RAY FLARES FROM SCATTERING SURFACES

With the exception of  $\alpha' \simeq 0$  photons, the last term in the square bracket of equation (15) is comparable to the sum of the first two and cannot be ignored. This prevents us to solve analytically for  $t_{fs}(t_{sc}, \alpha')$ , hence the analytical integration of the scattered emission is not possible either. Nevertheless, some properties of the scattered emission decay can be obtained by considering only the  $\alpha' = 0$  photons, i.e. photons which are emitted by the forward shock at angle  $\pi$  relative to its direction of motion and then scattered along the center-observer axis. For these photons, the last term in the square bracket of equation (15) can be ignored, leading to

$$t_{fs}(\alpha' = 0) = t_{sc} - \frac{1}{2}t_{lag}. \quad (26)$$

Because the scattered pre-deceleration emission is negligible, we can restrict attention to  $t_{fs} > t_0$ . Then, given that  $t_{sc} > t_{fs}$ , it follows that  $t_0 \gg t_{lag}$  ensures that  $t_{sc} \gg t_{lag}$ . For a Newtonian reverse shock, the lab-frame deceleration timescale corresponds to the mass swept-up by the forward shock reaching a fraction  $\gamma_0^{-1}$  of the ejecta, which leads to

$$(s = 0) \quad t_0 = 4.3 \times 10^6 (E_{sc,53}/n_0)^{1/3} (\gamma_0/100)^{-2/3} \text{ s} \quad (27)$$

$$(s = 2) \quad t_0 = 1.3 \times 10^5 (E_{sc,53}/A_*) (\gamma_0/100)^{-2} \text{ s} \quad (28)$$

hence the  $t_0 \gg t_{lag}$  condition sets an upper on the forward-shock's initial Lorentz factor:

$$(s = 0) \quad \gamma_0 < 10^6 (E_{sc,53}/n_0)^{1/2} (t_{lag}/10^4 \text{ s})^{-3/2} \quad (29)$$

$$(s = 2) \quad \gamma_0 < 360 (E_{sc,53}/A_*)^{1/2} (t_{lag}/10^4 \text{ s})^{-1/2}. \quad (30)$$

Anticipating the result that the scattered emission arrives at observer time  $T_{sc} \simeq t_{lag}$ , we have scaled  $t_{lag}$  to the latest time when X-ray flares are usually observed by the X-ray Telescope (XRT) on Swift. Thus, for  $\gamma_0$  satisfying condition (29) or (30),  $t_{sc} \gg t_{lag}$  is satisfied and  $t_{lag}$  can be ignored in the round bracket of equation (17) and in equation (26), leading to

$$t_{fs}(\alpha' = 0) \simeq t_{sc} \quad (31)$$

and

$$T_{sc} \simeq t_{lag} + \frac{t_{sc}}{2\Gamma^2} \simeq t_{lag} + \frac{t_{fs}}{2\Gamma^2} = t_{lag} + (4-s) \frac{\gamma^2(T_{fs})}{\Gamma^2} T_{fs} \quad (32)$$

where the last result follows from equation (20). Equation (32) relates the arrival-time of a forward-shock photon to when it would arrive if it were emitted backwards ( $\alpha = 0$  corresponds to angle  $\pi$  between the photon propagation direction and that of the forward shock) and then scattered. It allows the calculation of the range of arrival times for scattered photons, starting with the photons emitted by the forward shock at the onset of deceleration ( $T_0$ )

$$T_{sc}^{min} = t_{lag} + (4-s) \frac{\gamma_0^2}{\Gamma^2} T_0 \quad (33)$$

and until the scatterer catches-up with the forward shock. The latter is given by setting  $T_{fs} = T_{sc}$  in equation (32) which leads to

$$T_{sc}^{max} = t_{lag} + (4-s) \frac{\gamma^2(T_{sc})}{\Gamma^2} t_{lag} \quad (34)$$

where  $\gamma(T_{sc}) \ll \Gamma$  was assumed, which is ensured if  $\gamma_0 \ll \Gamma$ . The latter will always be the case considered here because only then the scattered emission can be brighter than that from the forward shock. Thus, for a forward-shock initial Lorentz factor well below that of the scattering surface, equations (33) and (34) show that the forward-shock photons left behind the shock and swept-up by the scatterer arrive at observer at  $T \simeq t_{lag}$  over a time interval  $\delta T \simeq (4-s)[\gamma^2(T)/\Gamma^2]t_{lag}$  which is much less than  $t_{lag}$ .

This means that the scattering of the forward shock emission by a surface of higher Lorentz factor can yield a flare of duration

$$\delta T \simeq (4-s) \frac{\gamma^2(T)}{\Gamma^2} T \ll T \quad (35)$$

much shorter than the age of the afterglow. Furthermore, that the flare from a scattering surface occurs at  $T \simeq t_{lag}$ , shows that, in the case of a radially-extended scattering outflow, the brightness of the scattered emission at observer time  $T$  reflects the properties (Lorentz factor  $\Gamma$ , mass distribution  $dM_{sc}/dt_{lag}$ ) of the scattered fluid ejected at lab-frame time  $t_{lag} = T$ , i.e. *the brightness of the scattered emission mirrors the scattering outflow properties in real time* (modulo cosmological time-dilation).

For the calculation of the scattered emission, we approximate  $\omega \simeq 0$  in equation (5), hence the Doppler factor for the forward-shock-scatterer relative motion is

$$D = \Gamma/\gamma. \quad (36)$$

This means that, in the frame of the scatterer, the forward-shock photons arrive within an angle  $D^{-1} = \gamma/\Gamma$  around the radial direction of motion. Scattering by electrons of the incoming photons redistribute them nearly isotropically, hence the comoving frame of the scattered radiation (equation 2) satisfies

$$I'_{sc} \simeq \tau_{sc} \frac{\pi(\gamma/\Gamma)^2}{4\pi} I'_{in}. \quad (37)$$

Substituting in equation (16), we obtain

$$F_{sc}(\nu, T_{sc}) \propto \Gamma \tau_{sc} \left(\frac{\gamma}{\Gamma}\right)^2 I'_{in}(\nu/\Gamma, t_{sc}) \quad (38)$$

which, after using equations (4) and (36), yields

$$F_{sc}(\nu, T_{sc}) \propto \tau_{sc} \frac{\Gamma^2}{\gamma} I'_{fs}(\nu\gamma/\Gamma^2, t_{sc}). \quad (39)$$

Then, with the aid of equation (18), we can write

$$\frac{F_{sc}(\nu, T_{sc})}{F_{fs}[\nu, T_{fs}(T_{sc})]} \simeq \tau_{sc}(T_{sc}) \frac{\Gamma^2}{\gamma^2(T_{fs})} \frac{I'_{fs}[\nu\gamma/\Gamma^2, t(T_{sc})]}{I'_{fs}[\nu/\gamma, t(T_{sc})]} \quad (40)$$

where we indicated that the forward-shock emission released at lab-frame time  $t(T_{sc})$  arrives at  $T_{sc}$  after being scattered and at time  $T_{fs}(T_{sc})$  if it is not scattered (the direct emission). In the simpler case when the forward-shock emission has a power-law spectrum between the two frequencies in the *rhs* of equation (40) (i.e. there are no spectral breaks in between),  $I'_{fs}(\nu) \propto (\nu')^{-\beta}$ , the ratio of intensities in that equation is  $(\Gamma/\gamma)^{2\beta}$ , thus

$$\frac{F_{sc}(\nu, T_{sc})}{F_{fs}[\nu, T_{fs}(T_{sc})]} \simeq \tau_{sc} \left(\frac{\Gamma}{\gamma}\right)^{2\beta+2}. \quad (41)$$

This result can also be derived from that the ratio of the spectral peak fluxes and peak frequencies of the flare and forward-shock emissions are

$$\frac{F_{sc}(\nu_p^{sc})}{F_{fs}(\nu_p^{fs})} = \tau_{sc} \frac{\Gamma^2}{\gamma^2}, \quad \frac{\nu_p^{sc}}{\nu_p^{fs}} = \frac{\Gamma^2}{\gamma^2} \quad (42)$$

and from that the forward-shock and scattered fluxes at a frequency  $\nu > \nu_p$  are given by  $F(\nu) = F_p(\nu/\nu_p)^{-\beta}$ . For either ratio of equation (42), one factor  $\Gamma/\gamma$  results from the relativistic motion of the sources toward the observer and another one is from the forward-shock-scatterer relative motion. For the peak flux ratio, the factor  $(\Gamma/\gamma)^2$  represents the time-contraction (the angular beaming part associated with the relative motion is lost because electron scattering makes the incoming radiation nearly isotropic, while the frequency Doppler boosts are lost because we are working with fluxes

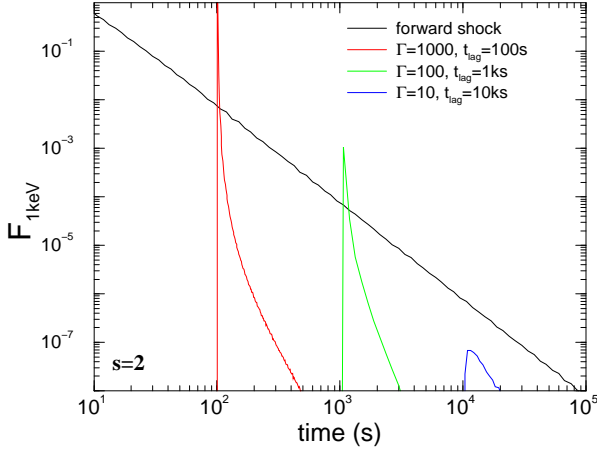


**Figure 3.** Forward-shock and scattered X-ray light-curves (in arbitrary units) from a scattering surface of Lorentz factor  $\Gamma$ , ejected at  $t_{lag}$  after the forward shock. The optical thickness to electron scattering of the reflecting surface is calculated from equation (3) for  $E_{sc} = 10^{53}$  erg and a purely leptonic composition ( $N_p = 0$ ). The Lorentz factor  $\gamma$  of the forward-shock is that given in equation (22) for  $E_{fs}/A_* = 10^{53}$  erg. The evolution of the forward-shock spectral properties are those of equations (24) and (25) for  $s = 2$ . The comoving-frame spectrum of the forward-shock emission is that given in the upper two lines of equation (23) with  $p = 3$ , observer-frame injection frequency  $h\nu_i(1s) = 100$  eV, and cooling frequency well above X-rays. Because  $\Gamma \gg \gamma$  for the earlier two flares, these flares (1) occur at an observer time equal to the lab-frame delay time between the forward shock and scatterer ejections, (2) last much shorter than the time when they occur, and (3) are brighter than the forward-shock emission.

per unit frequency). For the peak frequency ratio, the factor  $(\Gamma/\gamma)^2$  represents the relativistic Doppler effect.

Figure 3 shows the flares obtained numerically for a few values of the scattering surface Lorentz factors  $\Gamma$  and for a wind-like medium. It illustrates that the flare occurs at an observer time equal to the initial lag of the scattering surface behind the forward-shock (equations 33 and 34), lasting much shorter than the time when it occurs (equation 35), and being brighter than the underlying forward-shock emission for a larger  $\Gamma/\gamma$  Lorentz factor contrast (equation 41). This condition implies that the emission scattered along the observer-center line ( $\alpha = 0$ ) arrives at observer over a very short time (equation 35), hence the decay of the flare from a fast scattering surface is set by the geometrical curvature of the surface (photons emitted from fluid moving at increasing angles relative to observer arrive progressively later), which leads to a sharp rise and a  $F_{sc}(\nu) \propto (T_{sc} - t_{lag})^{-(\beta+2)}$  flare decay (Kumar & Panaitescu 2000). Other kinds of flare profiles can be obtained with a scattering outflow of radial extent  $\delta t_{lag} \gtrsim t_{lag}$  and adequate distributions for the scatterer Lorentz factor  $\Gamma(t_{lag})$  and mass  $dM_{sc}/dt_{lag}$  (§5.2).

#### 4 X-RAY PLATEAUS FROM SCATTERING OUTFLOWS – ANALYTICAL TREATMENT

To calculate from equation (40) the emission scattered by a radially-extended outflow with a  $dM/dt_{lag}$  radial mass-distribution, we discretize it as a sequence of scattering sur-

faces of mass  $\delta M = \delta t_{lag}(dM/dt_{lag})$  ejected at an interval  $\delta t_{lag}$  and add their scattered emissions. Thus, the optical thickness of the discretized outflow is

$$\tau_{sc}(T_{sc}) \propto \frac{\delta t_{lag}(dM/dt_{lag})}{R^2(T_{sc})} \quad (43)$$

where

$$R(T_{sc}) \simeq t_{sc} - t_{lag} \simeq 2\Gamma^2(T_{sc} - t_{lag}) \quad (44)$$

as can be inferred from equation (17) in the  $\Gamma \gg 1$  limit. The power-law spectrum of the forward-shock emission (equation 23) and the power-law evolution of its spectral characteristics (equation 25), lead to a received forward-shock emission that decays as a power-law in time

$$F_{fs}(\nu) \propto T^{-\alpha_{fs}} \quad (45)$$

where the index  $\alpha_{fs}$  is a linear function of the spectral slope  $\beta$  that will be specified later. By substituting equations (43), (44), and (45) in (40) we arrive at

$$F_{sc}(\nu, T_{sc}) \propto \frac{\delta t_{lag}(dM/dt_{lag})}{\Gamma^2\gamma^2(T_{sc} - t_{lag})^2} \frac{I'_{fs}(\nu\gamma/\Gamma^2)}{I'_{fs}(\nu/\gamma)} T_{fs}^{-\alpha_{fs}}. \quad (46)$$

From the first equation (20) and equation (31), and using  $t_{sc}$  obtained from equation (17) in the  $t_{sc} \gg t_{lag}$  limit (which is a good approximation), the arrival-time  $T_{fs}$  of the direct forward-shock emission corresponding to an arrival-time  $T_{sc}$  of the scattered photons is found to satisfy

$$T_{fs} \propto [\Gamma^2(T_{sc} - t_{lag})]^{4-s}. \quad (47)$$

For the scattered flux at time  $T$ , we integrate the flux from the scattering outflow element  $\delta M$  to obtain the fluence  $\Phi_{sc}(\nu, T)$  and divide it by the observer time-interval  $\delta T$  over which that fluence is spread. Taking into account the one-to-one correspondence between the lag time  $t_{lag}$  and the observer arrival-time  $T$  of scattered emission, we obtain that, for an extended scattering outflow,

$$F_{\nu}^{sc}(T) = \frac{1}{\delta t_{lag}} \int_{T_{sc}^{min}(T)}^{T_{sc}^{max}(T)} F_{sc}(\nu, T_{sc}) dT_{sc} \propto \frac{dM}{dT} \Gamma^{4-2s-(8-2s)\alpha_{fs}} \times \int_{T_{sc}^{min}(T)}^{T_{sc}^{max}(T)} (T_{sc} - t_{lag})^{1-s-(4-s)\alpha_{fs}} \frac{I'_{fs}(\nu\gamma/\Gamma^2)}{I'_{fs}(\nu/\gamma)} dT_{sc} \quad (48)$$

after using equations (46) and (47), with the forward-shock Lorentz factor from the second equation (20).

To continue, we have to specify the location of the two break frequencies (injection  $\nu'_i$  and cooling  $\nu'_c$ ) of the forward-shock synchrotron spectrum. The X-ray light-curve plateaus occur after about 1 ks, when the injection frequency is expected to be below X-rays ( $\nu'_i < \nu_x/\gamma$ ) even for equipartition electron and magnetic field parameters (for several afterglows, the optical spectral energy distribution at  $T < 1$  ks decreases with photon energy, thus  $\nu_i$  is even lower, below optical). The up-scattered injection frequency could be below or above X-rays. In the latter situation ( $\nu'_i > \nu_x\gamma/\Gamma^2$ ), we are interested only in the case where the up-scattered cooling frequency is below X-rays ( $\nu'_c < \nu_x\gamma/\Gamma^2$ ) because, in the opposite case, the up-scattered spectrum would be  $F_{\nu} \propto \nu^{1/3}$ , which has never been observed (afterglow spectra measured by XRT are softer than  $\nu^{-1/2}$ ).

$$4.1 \quad \nu'_i < \nu_x \gamma / \Gamma^2 < \nu_x / \gamma < \nu'_c$$

In this case,  $\nu_i^{fs} < \nu_x < \nu_c^{fs}$  and  $\nu_i^{sc} < \nu_x < \nu_c^{sc}$ , thus the spectral slopes of the forward-shock and scattered X-ray emissions are  $\beta_x^{fs} = \beta_x^{sc} = (p-1)/2$ , with  $p$  the exponent of the electron distribution with energy in the forward shock. The decay index of the forward-shock X-ray emission is

$$\alpha_{fs} = \frac{3}{2}\beta_x + \frac{s}{8-2s} \quad (49)$$

where  $\beta_x \equiv (p-1)/2$ .

The ratio of intensities in equation (48) is  $(\Gamma/\gamma)^{2\beta_x}$ , which, after using equations (33) and (34) for the integral limits, leads to

$$F_\nu^{sc}(T) \propto \frac{dM}{dT} \Gamma^{2\beta_x} \frac{1}{A} \{ [T\gamma^2(T)]^A - (T_0\gamma_0^2)^A \} \quad (50)$$

where

$$A = 2 - 1.5s - \beta_x(3 - 0.5s). \quad (51)$$

For  $\beta_x < \beta_0$  defined by

$$\beta_0 = \frac{4-3s}{6-s} = \begin{cases} 2/3 & s=0 \\ -1/2 & s=2 \end{cases} \quad (52)$$

the exponent  $A$  is positive and the scattered flux of equation (50) is dominated by the scattering of forward-shock emission at  $T_{sc} \lesssim T$ . Taking into account that  $T\gamma^2(T) \propto T^{1/(4-s)}$ , it follows that

$$F_\nu^{sc}(T) \propto \frac{dM}{dT} \Gamma^{2\beta_x} T^{A/(4-s)} = \frac{dM}{dT} \Gamma^{2\beta_x} \begin{cases} T^{-(3\beta_x-2)/4} & s=0 \\ T^{-(\beta_x+1/2)} & s=2 \end{cases} \quad (53)$$

For  $\beta_x > \beta_0$ ,  $A$  is negative and the scattered flux is dominated by the scattering of photons produced by the forward shock around the deceleration time. In this case, (50) leads to

$$F_\nu^{sc}(T) \propto \frac{dM}{dT} \Gamma^{2\beta_x} \quad (54)$$

which is, evidently, independent of the ensuing decay of the forward-shock emission.

$$4.2 \quad \nu'_i < \nu_x \gamma / \Gamma^2 < \nu'_c < \nu_x / \gamma$$

This case corresponds to  $\nu_i^{fs} < \nu_c^{fs} < \nu_x$  and  $\nu_i^{sc} < \nu_x < \nu_c^{sc}$ , for which  $\beta_x^{fs} = p/2$ ,  $\beta_x^{sc} = (p-1)/2$  and

$$\alpha_{fs} = \frac{1}{4}(6\beta_x + 1) \quad (55)$$

independent of the circumburst medium stratification, where  $\beta_x \equiv (p-1)/2$  (i.e.  $\beta_x$  is the slope of the up-scattered spectrum, which is what XRT would measure if the scattered emission were brighter than forward-shock's). The ratio of intensities in equation (48) is  $(\Gamma/\gamma)^{2\beta_x} (\nu/\gamma\nu'_c)^{1/2}$ , leading to the same light-curves of the scattered emission as given in equations (53) and (54), with  $\beta_0$  of equation (52).

$$4.3 \quad \nu'_i, \nu'_c < \nu_x \gamma / \Gamma^2 < \nu_x / \gamma$$

This is the  $\nu_i^{fs}, \nu_c^{fs} < \nu_x$  and  $\nu_i^{sc}, \nu_c^{sc} < \nu_x$  case, for which  $\beta_x^{fs} = \beta_x^{sc} = p/2$  and

$$\alpha_{fs} = \frac{1}{2}(3\beta_x - 1) \quad (56)$$

with  $\beta_x \equiv p/2$ . The intensity ratio of equation (48) is  $(\Gamma/\gamma)^{2\beta_x}$ , leading to a scattered flux as given in equation (50) with the exponent

$$A = 4 - 1.5s - \beta_x(3 - 0.5s) \quad (57)$$

thus

$$\beta_0 = \frac{8-3s}{6-s} = \begin{cases} 4/3 & s=0 \\ 1/2 & s=2 \end{cases} \quad (58)$$

For  $\beta_x < \beta_0$ , the light-curve of the scattered emission is

$$F_\nu^{sc}(T) \propto \frac{dM}{dT} \Gamma^{2\beta_x} \begin{cases} T^{-(3/4)\beta_x+1} & s=0 \\ T^{-\beta_x+1/2} & s=2 \end{cases} \quad (59)$$

For  $\beta_x > \beta_0$ , the scattered emission satisfies equation (54).

$$4.4 \quad \nu'_c < \nu_x \gamma / \Gamma^2 < \nu'_i < \nu_x / \gamma$$

In this case ( $\nu_i^{fs}, \nu_c^{fs} < \nu_x$  and  $\nu_c^{sc} < \nu_x < \nu_i^{sc}$ ), we have  $\beta_x^{fs} = p/2$ ,  $\beta_x^{sc} = 1/2$ , and  $\alpha_{fs}$  is given by equation (56). The intensity ratio in equation (48) is  $(\Gamma/\gamma)(\nu/\gamma\nu'_i)^{\beta_x-1/2}$ , leading to

$$F_\nu^{sc}(T) \propto \frac{dM}{dT} \Gamma \begin{cases} T^{5/8} & s=0 \\ T^0 & s=2 \end{cases} \quad (60)$$

## 5 SCATTERED EMISSION – NUMERICAL RESULTS

The above analytical derivations for the scattered emission light-curve were made for photons moving along the explosion center – observer axis, for which equation (15) can be solved, yielding the trivial solution of equation (31),  $t_{fs} \simeq t_{sc}$ . For other photons ( $\alpha' > 0$ ), the Doppler factor of the scatterer–forward-shock relative motion is of the same order,  $D \simeq \Gamma/\gamma(t_{fs})$ , but the retarded emission time cannot be obtained analytically.

The scattered emission from a radially-extended outflow is calculated numerically by discretizing it into surfaces and by using the relevant equations of §2– §4 to calculate the emission from each surface. We have verified that (1) the decays given in equations (53) and (59) (obtained in the  $\alpha' = 0$  approximation) are correct and (2) the decay of the scattered light-curve is independent of the incident spectrum for softer spectra (i.e. independent of the decay of the forward-shock emission). Therefore, as expected analytically, there is a "critical" spectral slope  $\beta_0$  of the forward-shock emission such that the scattered flux received at some time  $T$  is mostly that produced by the forward shock at same time  $T$ , if  $\beta < \beta_0$ , or at the onset of deceleration, if  $\beta > \beta_0$ . However, the numerical integration of the scattered flux leads to a  $\beta_0$  that is larger than that given in equations (52) and (58) by  $\sim 1$ .

For the case presented in §4.1, we find numerically that  $\beta_0 \simeq 2$  for  $s = 0$  and  $\beta_0 \simeq 0.5$  for  $s = 2$  (the dependence of the scattered emission decay on the incident spectrum is shown in Figure 4), while for that of §4.3,  $\beta_0 \simeq 2.5$  for  $s = 0$  and  $\beta_0 \simeq 1.5$  for  $s = 2$ . As the X-ray spectral slopes measured by XRT are between 0.5 and 1.5, the decay of the X-ray plateau resulting from scattering the forward-shock

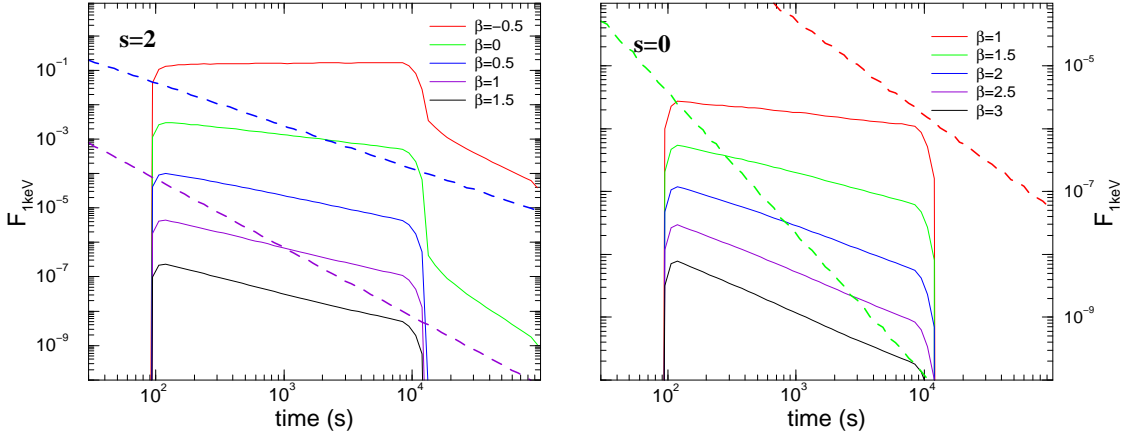


**Figure 4.** X-ray light-curves (flux in arbitrary units) from the forward-shock (thick lines) and a radially-extended scattering outflow (thin lines), for various slopes  $\beta$  of the forward-shock emission spectrum. The dynamics of this shock is given by  $E_{fs}/A_* = 10^{53}$  erg in the left panel (for a wind-like medium,  $s = 2$ ) and  $E_{fs}/n = 10^{53}$  erg cm<sup>3</sup> in the right panel (for a homogeneous circumburst medium,  $s = 0$ ). The cooling frequency of the forward-shock synchrotron emission is set above X-rays and injection frequency is  $h\nu_i(1s) = 1$  eV. The brightness of the forward-shock emission decreases strongly with increasing spectral slope. The scattering outflow has  $E_{sc} = 10^{53}$  erg, a constant Lorentz factor  $\Gamma$  ( $10^3$  for left panel,  $10^4$  for right panel), constant mass ejection rate  $dM/dt_{lag}$ , is purely leptonic, and was ejected from 100 s to 10 ks after the forward-shock (hence the scattered emission arrives at observer at 0.1–10 ks). Some of the spectral slopes are unrealistically soft or hard – XRT measures  $\beta_x \in (0.5, 1.5)$  – but have been used to show that the decay of the scattered emission depends on  $\beta$  if the forward-shock emission is hard, becoming independent of  $\beta$  if the forward-shock emission is soft. The transition between these two regimes takes place at  $\beta_0 \simeq 0.5$  for  $s = 2$  and at  $\beta_0 \simeq 2$  for  $s = 0$ . The scattered emission shown in the left panel after 10 ks (for the two hardest spectra) is the “large-angle emission”, arriving from the fluid moving at angle  $\gg \Gamma^{-1}$  relative to the direction toward the observer.

emission should be independent of  $\beta_x$  only if (1) the circumburst medium is a wind, (2)  $\nu_i^{fs} < \nu_x < \nu_c^{fs}$ , and (3)  $\nu_i^{sc} < \nu_x < \nu_c^{sc}$ . In all other cases, the decay of the scattered emission is correlated with the spectral slope  $\beta_x$ .

For the parameters used in Figure 4, the scattered emission is brighter than the forward-shock’s (and yields a light-curve plateau) only if the spectrum of the forward-shock emission is softer than  $\beta \simeq 1.2$  for  $s = 0$  and  $\beta \simeq 0.8$  for  $s = 2$ . Numerically, we find that X-ray plateaus can be obtained for harder forward-shock emissions (down to the hardest observed XRT spectra –  $\beta_x \simeq 0.5$ ) if (1) the cooling frequency of the forward-shock emission is below X-rays and the up-scattered cooling frequency above, (2) the Lorentz factor or energy of the scattering outflow is larger, or (3) the scattering electrons are relativistic (i.e. they inverse-Compton scatter the incoming photons).

### 5.1 Chromatic plateaus and breaks

As illustrated in Figure 5, the up-scattered emission may overshine the forward-shock’s only at higher photon energies (in the X-rays) but not at lower frequencies (e.g. in the optical). This implies that the X-ray plateau produced by scattered forward-shock emission does not appear in the optical. Consequently, the end of the plateau will also be a chromatic feature. Such chromatic light-curve breaks are observed for several GRB afterglows: GRB 050401 (Watson et al 2006 - Figure 1); GRBs 050319, 050607, 050713A, 050802, 050922C (Panaitescu et al 2006b); GRB 070110 (Troja et al 2007 - Figure 1), GRB 050318 (Liang et al 2007) and, as noted before, cannot be accommodated by the forward-shock emission alone.

### 5.2 Diversity of plateau decays and flare shapes

In Figure 6, we compare the light-curve decay indices and spectral slopes measured by XRT during the X-ray plateau with the analytical results of equations (53) and (59) for a constant mass-flux  $dM/dt_{lag}$  and Lorentz factor  $\Gamma$  of the scattering outflow, using the  $\beta_0$  derived numerically (instead of that given in equations 52 and 58 for the central line-of-sight photons).

The spectral slopes displayed in Figure 6 show that the afterglows without plateaus (i.e. those for which the forward-shock emission is brighter than the scattered emission at all times) are generally harder than the afterglows with plateaus. This confirms the expectation illustrated in Figure 4 for the scattering-outflow model, that plateaus are easier to obtain if the forward-shock emission is softer (as this leads to a faster-decaying forward-shock light-curve).

Although most of the afterglow decays displayed in Figure 6 are in the  $\alpha_x < 1$  region, where the decay index  $\alpha_x$  depends on the spectral slope  $\beta_x$ , these two quantities are not correlated (linear correlation coefficient  $r(\alpha_x, \beta_x) = 0.03 \pm 0.10$ ). This can be due either to that all cases analyzed in §4.1–§4.3 occur in reality or to that  $dM/dt_{lag}$  and  $\Gamma$  vary with ejection time  $t_{lag}$  (which is measured directly by the observer time) for some/most afterglows.

For a power-law radial distribution of the scattering outflow mass-flux ( $dM/dt_{lag} \propto t_{lag}^{-m}$ ) and Lorentz factor ( $\Gamma \propto t_{lag}^{-g}$ , with  $g \geq 0$  because internal shocks lead to a Lorentz factor decreasing outward), the decay index  $\alpha_{sc}$  of the scattered emission is

$$\alpha_{sc} = m + 2g\beta_x + \alpha_{sc}(m=0, g=0) \quad (61)$$

with  $\alpha_{sc}(m=0, g=0)$  being the decay index given in equations (53), (54), (59), and (60) for a uniform outflow.



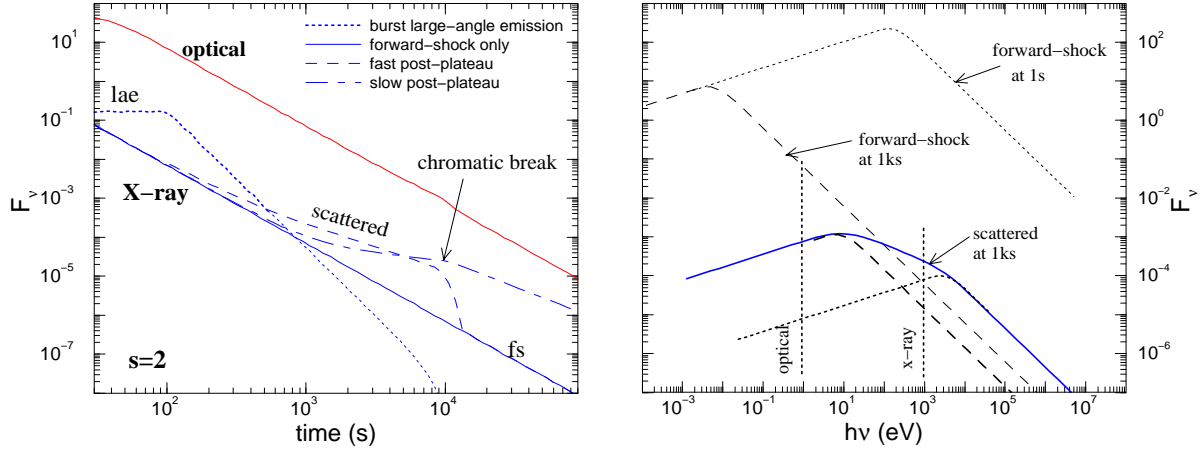


**Figure 5.** Light-curves and spectra of forward-shock and scattered emissions. *Right panel:* spectrum of synchrotron forward-shock emission at 1 s and 1 ks and spectrum of up-scattered emission at 1 ks. Thick lines show the 1s (dotted) and 1 ks (dashed) spectra of the up-scattered forward-shock emissions, shifted vertically toward the integrated spectrum to match their expected peak frequencies. Note that the scattered emission is brighter than the forward-shock’s in the X-ray but not in the optical, which leads to a decoupling of the two light-curves and to chromatic X-ray breaks. Also, note that the scattered emission may be harder in the X-rays than the underlying forward-shock spectrum. *Left panel:* chromatic X-ray light-curve breaks produced by the scattered emission. At early times, the X-ray afterglow emission is dominated by the “large-angle” prompt emission released during the burst but arriving later at observer (owing to the spherical curvature of the emitting surface). The decay of the X-ray emission reflects the distribution of mass  $dM/dt_{lag}$  and Lorentz factor  $\Gamma$  in the scattering outflow with geometrical depth  $ct_{lag}$  (distance from forward-shock): if either  $dM/dt_{lag}$  or  $\Gamma(t_{lag})$  fall sharply at some distance  $ct_{break}$  then the X-ray break at observer time  $t_{break}$  will be very sharp (dashed line), as observed for a minority of Swift afterglows; a more gradual decrease of  $dM/dt_{lag}$  or  $\Gamma(t_{lag})$  at  $t_{lag} > t_{break}$  yields a steepening of the X-ray decay at  $t_{break}$  (dot-dashed curve), as displayed by a majority of Swift afterglows. *Parameters.* Forward-shock:  $E_{fs}/A_* = 10^{53}$  erg (wind-like medium);  $\beta = 1$ ,  $h\nu_i(1s) = 100$  eV,  $\nu_c$  above X-rays. Scattering outflow: uniform  $\Gamma = 10^3$ , baryon-free composition,  $t_{break} = 10$  ks, and (1)  $E_{sc} = 10^{53}$  erg,  $dM/dt_{lag} = 0$ , cold outflow, ending at  $t_{break}$  for the X-ray light-curve with a sharp plateau end, (2)  $E_{sc} = 10^{54}$  erg,  $dM/dt_{lag} \propto t_{lag}^{1/2}$  for  $t_{lag} < t_{break}$ ,  $dM/dt_{lag} \propto t_{lag}^{-1/2}$  for  $t_{lag} > t_{break}$ , hot outflow with  $\gamma_e = 10$  for the X-ray light-curve with a slow post-plateau decay. The optical flux is the same for both scattering outflow parameters because the scattered emission is dimmer than the forward-shock’s.

Therefore, a variety of X-ray plateau decays can be obtained by varying the indices  $m$  and  $g$  of equation (61). The same applies to the shape of the flares resulting from up-scattering the forward-shock emission (Figure 7). In particular, decreasing  $dM/dt_{lag}$  or  $\Gamma(t_{lag})$  yield flares with a slow fall, while an increasing  $dM/dt_{lag}$  produces flares with a slow rise, which can account for the diverse morphology of X-ray flares identified by Chincarini et al (2007).

### 5.3 Fast post-plateau decays

Given that the post-plateau X-ray decay depends on the  $dM/dt_{lag}$  and  $\Gamma(t_{lag})$  distributions at  $t_{lag} > t_{break}$ , the scattering outflow model can account (Figure 5) for the extremely fast-decaying  $F_x \propto T^{-8\pm 2}$  post-plateau emission observed for GRB afterglow 070110 (Troja et al 2007) after 20 ks and the  $F_\nu \propto T^{-3}$  post-plateau decays of GRBs 050730 (Perri et al 2007), 060413, and 060607A (Molinari et al 2007, Nysewander et al 2007) after 10 ks, and of GRB 070311 (Guidorzi et al 2007) after 150 ks. If the scattering outflow is concentrated in thin shells then the same model can account for the fast decay of the afterglow emission after flaring episodes, followed by a smooth and slower decay (from the emergent forward-shock emission), as observed for GRB afterglow 051117A (Goat et al 2007) at 10 ks. Such fast decays cannot be explained by the standard forward-shock model.

After the X-ray plateau, the majority of afterglows ex-

hibit a light-curve decay  $F_x \propto t^{-\alpha}$  with  $\alpha \in (1, 2)$ . This indicates that  $dM/dt_{lag}$  and  $\Gamma(t_{lag})$  are nearly uniform distributed (i.e. the indices  $m$  and  $g$  of equation 61 are not far from zero) and that large values of these parameters, mimicking a sharp cut-off in their distribution and yielding sharp post-plateau decays, are rare. Figure 5 (left panel) illustrates the chromatic X-ray break, followed by a slow post-plateau decay, that is obtained with a broken power-law for  $dM/dt_{lag}$ , the transition between the two power-laws being made at the epoch of the X-ray break.

### 5.4 Spectral evolution of flares and plateaus

Figure 5 (right panel) also shows that scattering of the forward-shock emission may yield a spectrum with a turnover extending up to (or above) the X-ray range, thus the scattered emission may be harder than the intrinsic forward-shock emission. This implies that, sometimes, X-ray plateaus and flares could be harder than the preceding and following X-ray emission. A spectral softening at the end of plateau is not observed (in general), which indicates that either the spectral turn-over formed by up-scattering the peak frequency of the synchrotron forward-shock emission lies below the X-ray or that it is in the X-rays but does not evolve. In the latter case, the break at the end of plateau should be attributed to a change in the distribution of outflowing mass with depth, as the alternative explanation – a decreasing outflow Lorentz factor – would produce

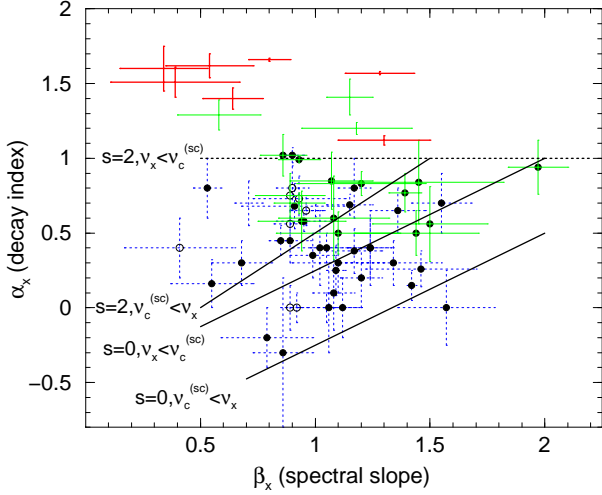


**Figure 6.** Power-law decay index of the X-ray plateau ( $F_\nu \propto T^{-\alpha_x}$ ) vs. spectral slope ( $F_\nu \propto \nu^{-\beta_x}$ ) for 40 Swift afterglows with flattening followed by a steepening of the X-ray light-curve at 1–30 ks (blue, dotted error bars). Also shown are 7 afterglows with a single power-law X-ray light-curve decay after burst and until 10–100 ks (red, thick error bars), and 17 afterglows with a flattening of the X-ray light-curve after burst tail but without a steepening observed until last observation, days after trigger (green, thin error bars). Lines show the model expectations for the scattered forward-shock emission model (equations 53 and 59) for a constant mass-flux ( $d^2M/dt_{lag}^2 = 0$ ) and Lorentz factor ( $d\Gamma/dt_{lag} = 0$ ) of the scattering outflow. The range of model decay indices expected is comparable to that observed for the 57 afterglows with an X-ray plateau (whether or not the plateau end was observed). 75 percent (filled symbols) and 90 percent (all symbols) of afterglows are consistent within  $1\sigma$  and  $2\sigma$ , respectively, with this model, thus 10–25 percent of afterglows require scattering outflows with non-constant  $dM/dt_{lag}$  and/or  $\Gamma(t_{lag})$ . Note that the 7 X-ray afterglows without slow decays are, on average, harder than the 57 afterglows with slow fall-offs, as expected for the scattering-outflow model.

a softening of the peak energy of the up-scattered spectrum (equation 42).

A hardening of the X-ray spectrum, followed by softening, is observed for the flares of GRB 050502B (Falcone et al 2006) and, perhaps, those of GRB 050904 (Cusumano et al 2007) occurring *during the afterglow phase*, which suggests that the turn-over at the peak of the up-scattered emission spectrum reaches sometimes the 0.3–10 keV range. This is consistent with flares originating from regions in the scattering outflow of Lorentz factor larger than the average (i.e. than for the part of the outflow yielding the plateau), although it is possible that the spectral peak energy of the flaring emission is larger than that of the plateau’s simply because flares occur at earlier times, when the peak frequency of the seed forward-shock emission is higher.

### 5.5 Cold and hot scattering outflows

If the scattering electrons are relativistic (with random Lorentz factor  $\gamma_e$  in the scattering outflow’s frame), they will inverse-Compton scatter the incident photon and increase its energy by a factor  $\simeq \gamma_e^2$  (in the frame of the scattering fluid). Then, the comoving intensity in the numerator of the

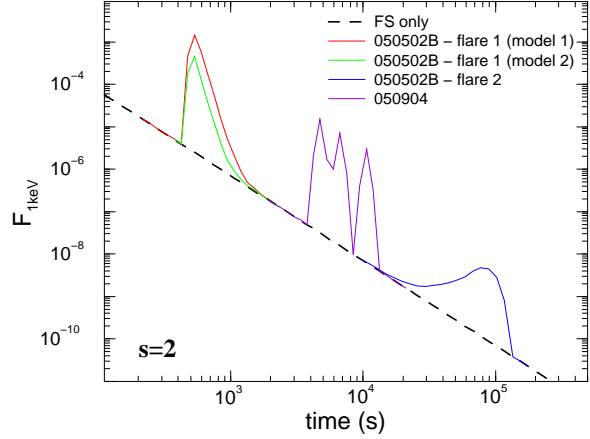


**Figure 7.** Flaring episodes for the scattered forward-shock emission obtained with fast evolving functions for the mass-flux  $dM/dt_{lag}$  and Lorentz  $\Gamma(t_{lag})$ , chosen so that the X-ray flares have a morphology resembling those of the flares of the afterglows indicated in legend (see Figure 1). The lab-frame timing of the scattering outflow ejection can be read directly from the observer time. General parameters:  $E_{fs}/A_* = 10^{53}$  erg (wind-like medium),  $\beta = 1$ ,  $h\nu_i(1s) = 1$  eV,  $\nu_c$  above X-rays;  $E_{sc} = 10^{53}$  erg, baryon-free composition. Other parameters: (1) model 1 for first flare of GRB 050502B –  $d^2M/dt_{lag}^2 = 0$ ,  $\Gamma = 10^4(t_{lag}/500s)^{-5}$ ; (2) model 2 for first flare of GRB 050502B –  $dM/dt_{lag} \propto t_{lag}^{-10}$ ,  $\Gamma = 10^4$  (constant); (3) second flare of GRB 050502B –  $dM/dt_{lag} \propto t_{lag}^3$ ,  $\Gamma = 3000$ ; (4) GRB 050904 –  $dM/dt_{lag} \propto t_{lag}^{-1}$ ,  $\Gamma = 10^4$  (3 episodes of ejection).

*rhs* of equation (40) is calculated at comoving frequency  $\nu\gamma/(\Gamma\gamma_e)^2$ . If this frequency is above the peak frequency of the synchrotron forward-shock emission (in the shock’s frame), then the scattered flux will be a factor  $\gamma_e^{2\beta_x}$  larger than that obtained for a cold outflow (equations 53, 54, and 59).

Hence, the decrease of the scattered flux by factor  $m_p/m_e = 1837$  resulting from going from a cold and purely-leptonic scattering outflow (as considered so far) to one with a unity baryon-to-lepton ratio can be compensated for if the latter is hot, so that the incident photons are inverse-Compton scattered off electrons with  $\gamma_e = (m_p/m_e)^{0.5/\beta_x}$ . This holds true as long as all incident photons up-scattered to observer frequency  $\nu$  are (before being scattered) above the peak frequency of the forward-shock synchrotron spectrum. For  $\beta_x > 1/2$  (as observed), it follows that  $\gamma_e < m_p/m_e$ , which implies that the internal shocks energizing the scattering outflow need not be relativistic and the necessary  $\gamma_e$  could be produced by small fluctuations in the Lorentz factor of the scattering outflow.

Alternatively, that  $F_{sc}(\nu) \propto (\Gamma\gamma_e)^{2\beta_x}$  implies that a hot, scattering outflow of bulk Lorentz factor  $\Gamma/\gamma_e$  and comoving-frame electron energy  $\gamma_e m_e c^2$  yields the same X-ray scattered flux as a cold outflow of Lorentz factor  $\Gamma$ . Thus, if the scattering outflow is hot, then an X-ray plateau can be obtained for a Lorentz factor  $\Gamma$  smaller than that considered for Figures 3, 4, 5, and 7.

## 5.6 Circumburst medium

For a given scatterer Lorentz factor  $\Gamma$  and forward-shock spectral slope  $\beta$ , a wind-like circumburst medium is more likely to yield an X-ray scattered emission brighter than the forward-shock's. This is primarily due to that, at a fixed observer time, the Lorentz factor of the forward-shock is lower for a wind-like medium than for a homogeneous one, as shown by equations (21) and (22), hence the scattering has a stronger effect (quantified by the ratio  $\Gamma/\gamma$ ) for the former case. Comparable forward-shock Lorentz factors would require a much higher homogeneous medium density ( $n \simeq 10^4 \text{ cm}^{-3}$ ), which is at odds with the low synchrotron self-absorption frequency (below 10 GHz), or a much lower wind density ( $A_* \simeq 0.01$ ), which is  $> 30$  times less tenuous than measured for Galactic WR stars.

A second reason for which the scattered emission is more prominent for a wind-like medium is at work when the cooling frequency of the forward-shock emission is above X-rays: in this case, the forward-shock flux decreases faster for a wind-like medium, allowing the scattered emission to emerge. Therefore, the scattering-outflow model for the X-ray plateaus favours a circumburst medium with the  $r^{-2}$  radial stratification expected for a massive star as the GRB progenitor.

However, we note that, if the scattering electrons are relativistic, then the ratio of scattered and direct fluxes is quantified by  $\Gamma\gamma_e/\gamma$ , thus a hotter scattering outflow could compensate for the above two factors which favour a wind-like medium.

## 6 CONCLUSIONS

The results presented in preceding sections illustrate that the up-scattering of the forward-shock emission by a more relativistic, lepton-enhanced outflow can accommodate four puzzling X-ray features discovered by Swift: flares, plateaus, chromatic light-curve breaks, and sharp post-plateau decays. The model requires the existence of a long-lived engine that releases relativistic ejecta for at least 10 ks or some other way of producing a relativistic outflow that has such a radial spread. That the scattering outflow has a higher Lorentz factor than the forward shock need not be a feature of the engine and could be just the consequence of the deceleration that the forward shock undergoes as it sweeps-up and energizes the ambient medium. The requirement that the scattering outflow is pair-rich is to ensure a sufficiently large (sub-unity) optical thickness to electron scattering, so that the scattered emission can overshine the forward-shock's direct emission and explain the above three features of X-ray afterglows. This requirement can be relaxed if the scattering outflow is hot (by birth or due to internal shocks), so that the incident photons are also inverse-Compton scattered (in addition to their bulk up-scattering).

Of the above-mentioned X-ray features, only plateaus can be explained by the forward-shock model: energy injection in this shock by means of some delayed ejecta should lead to a slower decay of the forward-shock emission. However, the other three features (flares, chromatic breaks, and sharp post-plateau fall-offs) cannot be accounted for by the forward-shock model, where fluctuation timescales are ex-

pected to be of order of the afterglow age and the multi-wavelength light-curve behaviours should be well coupled.

### 6.1 X-ray flares

The light-curves for the scattered forward-shock emission shown in Figure (7) show that this model can account for the sharpness and brightness of the flares observed in many X-ray afterglows. The dynamics of sweeping-up the photons left behind by the forward shock leads to flares of duration  $\delta T = (\gamma/\Gamma)^2 T$ , with  $\gamma$  and  $\Gamma$  the forward-shock Lorentz factor at observer time  $T$  and  $\Gamma$  that of the scatterer. This  $\delta T$  is also the spread in the photon-arrival time caused by the spherical curvature of the scattering surface:  $\delta T \simeq R/\Gamma^2 \simeq (\gamma^2 T)/\Gamma^2$ , where  $R \simeq \gamma^2 T$  is the radius of the scatterer when it catches-up with the forward shock. Therefore, very short flares are a natural feature of the scattered emission, provided that the radial spread of the scattering outflow is sufficiently small (instantaneous ejection). For longer-lived flares, the shape of the flare (fast-rise, fast-fall, or symmetric flares) depends on the radial distribution of the mass-flux  $dM/dt_{lag}$  and/or of the Lorentz factor  $\Gamma(t_{lag})$  in the scattering outflow (Figure 7).

### 6.2 X-ray plateaus, chromatic breaks, and sharp post-plateau decays

Figure 4 illustrates that X-ray plateaus (as observed for most afterglows) can result from scattering the forward-shock emission. Because the up-scattered emission is more likely to overshine the direct forward-shock emission at higher photon energies than at lower energies, this model can also produce chromatic plateaus and breaks, which appear in the X-rays but not in the optical as well (Figure 5). Such chromatic X-ray breaks are observed for several GRB afterglows.

Sharp decays following X-ray plateaus, as observed for a few GRB afterglows, result if the  $dM/dt_{lag}$  or  $\Gamma(t_{lag})$  of the scattering outflow decrease sufficiently fast at some point behind the forward shock (i.e. the scattering outflow has a well-defined trailing edge). Only a few XRT afterglows display a sharp post-plateau decay, the norm being that of a smooth transition to a steeper power-law decay. This requires scattering outflows with a more complex structure, where the plateau end corresponds to a change in the radial distribution of  $dM/dt_{lag}$  and/or  $\Gamma(t_{lag})$ . That most post-plateau X-ray light-curves have a slow decay indicates that the radial distributions of  $dM/dt_{lag}$  and  $\Gamma(t_{lag})$  (equation 61) are not far from being uniform and that they rarely exhibit the fast decrease with distance from the forward-shock that is required by the minority of X-ray afterglows with sharp post-plateau decays.

### 6.3 Prolonged activity of central engine

For a scattering outflow of Lorentz factor well above that of the forward shock, the arrival time of the scattered photons is nearly equal to the delay (in the lab frame) between the ejection of the forward-shock driving ejecta and the scattering fluid. This has two consequences. *First*, in addition to the spectral slope of the forward-shock emission, the scattered flux received at an observer time  $T$  reflects the prop-

erties ( $dM/dt_{lag}$  and  $\Gamma(t_{lag})$ ) of the scattering fluid ejected at lab-frame time  $t_{lag} = T$ . This implies that a variety of X-ray plateau decays and shapes can be obtained by choosing the right functions for  $dM/dt_{lag}$  and  $\Gamma(t_{lag})$  (equations 53, 54, 59, and 60). The *second* is that a flare seen at time  $T$  or a plateau lasting until  $T$  require that the central engine operates at/until a lab-frame time equal to  $T$ . Thus, the scattering-outflow model for X-ray flares and plateaus is still based on the existence of a long-lived engine, as is the internal-shock interpretation of flares.

#### 6.4 Scattering outflow vs forward shock

The post-plateau decay of Swift X-ray afterglows is generally compatible with a forward-shock origin (see fig. 5 of Willingale et al 2007, fig. 11 of Panaitescu 2007, fig. 6 of Liang et al 2007). However, no single variant of that model that can account for the spread of post-plateau decay indices for a given spectral slope. Furthermore, for a set of 60 Swift afterglows, we find that the post-plateau X-ray decay index is not correlated with the spectral slope (linear correlation coefficient  $r = -0.18 \pm 0.10$ ), contrary to what is expected for the forward-shock emission.

That lack of correlation is a natural consequence of the scattering model, where the post-plateau decay is determined not only by the spectral slope of the forward-shock seed photons but also by the radial distribution of  $dM/dt_{lag}$  and/or  $\Gamma(t_{lag})$  in the scattering outflow. A stronger argument in favour of this model for X-ray afterglows is that it can explain two features (chromatic light-curve breaks and sharp post-plateau decays) that cannot be accounted for by the forward-shock model.

However, about 30 percent of the well-monitored X-ray afterglows of Willingale (2007) do not have a plateau, thus their emission need not be attributed to a scattering outflow, and could originate in the forward shock. Furthermore, the GRB afterglows 051109A (Yost et al 2007), 060614 (Mangano et al 2007a), 060714 (Krimm et al 2007), and 060729 (Grupe et al 2007) display an achromatic break, which is seen simultaneously in the optical and X-ray light-curves. Such breaks require that both emissions arise from the same mechanism. Although that could be achieved by the scattering outflow model, provided that the forward-shock emission peaks at a sufficiently low energy that the scattered flux is dominant also in the optical, it seems more natural to attribute the achromatic breaks at plateau ends to the cessation of energy injection into the forward shock.

The forward-shock is also a more plausible origin for the long-lived, power-law X-ray afterglows of e.g. GRB 050416A (Mangano et al 2007b), GRB 050822 (Godet et al 2007), GRB 060319 (Burrows & Racusin 2007) GRB 060729, which, in the scattering outflow model, would require a central engine producing a scattering outflow with a nearly uniform distribution of  $dM/dt_{lag}$  and  $\Gamma$  over very long times ( $\lesssim 1$  Ms in source frame).

Therefore, the features of optical and X-ray afterglow light-curves provide evidence in favour of both the forward-shock and scattering-outflow models. When the forward-shock emission is the brightest, the X-ray afterglow may lack a plateau or, if it has one owing to energy injection in the blast-wave, then the plateau ends with an achromatic break. If the scattered emission is dominant, then the X-

ray afterglow exhibits a plateau, most likely ending with a chromatic break. This picture is supported by that X-ray afterglows without plateaus are harder (Figure 6), as a harder forward-shock emission is expected to be brighter and, thus, more likely to overshadow the scattered emission.

Thus, the observed diversity of Swift X-ray afterglows is due to both mechanisms being at work, in addition to the diversity that each model can produce on its own.

#### ACKNOWLEDGMENTS

This work was supported by NASA Swift Guest Investigator grant NNG06EN001

#### REFERENCES

- Burrows D. et al, 2007, *Phil Trans A*, 365, 1213  
 Burrows D., Racusin J., 2007, *Nuovo Cimento B*, 121, 1273  
 Chincarini G. et al, 2007, *ApJ*, submitted (astro-ph/0702371)  
 Cusumano G. et al, 2007, *A&A*, 462, 73  
 Falcone A. et al, 2006, *ApJ*, 641, 1010  
 Fan Y., Piran T., 2006, *MNRAS*, 197, 206  
 Fenimore E., Ramirez-Ruiz E., 1999, preprint (astro-ph/9909299)  
 Genet F., Daigne F., Mochkovitch R., 2007, *MNRAS*, 381, 732  
 Goad M. et al, 2007, *A&A*, 468, 103  
 Godet O. et al, 2007, *A&A*, 471, 385  
 Grupe D. et al, 2007, *ApJ*, 662, 443  
 Guidorzi C. et al, 2007, *A&A*, accepted (arXiv:0708.1383)  
 Ioka K. et al, 2006, *A&A*, 458, 7  
 Krimm H. et al, 2007, *ApJ*, 665, 554  
 Kumar P., Panaitescu A., 2000, *ApJ*, 541, L51  
 Kumar P. et al, 2007, *MNRAS*, 367, L52  
 Liang E., Zhang B-B., Zhang B., 2007, *ApJ*, accepted (arXiv:0705.1373)  
 Lyutikov M., 2006, *New J. of Phys.*, 8, 119  
 Mangano V. et al, 2007a, *A&A*, 470, 105  
 Mangano V. et al, 2007b, *ApJ*, 654, 403  
 Mészáros P., Rees M., 1997, *ApJ*, 476, 232  
 Molinari E. et al, 2007, *A&A*, 469, L14  
 Nousek J. et al, 2006, *ApJ*, 642, 389  
 Nysewander M. et al, 2007, *ApJ*, submitted (arXiv:0708.3444)  
 Paczyński B., Rhoads J., 1993, *ApJ*, 418, L5  
 Panaitescu A. et al, 2006a, *MNRAS*, 366, 1357  
 Panaitescu A. et al, 2006b, *MNRAS*, 369, 2059  
 Panaitescu A. et al, 2007, *MNRAS*, 379, 331  
 Perri M. et al, 2007, *A&A*, 471, 83  
 Ramirez-Ruiz E., Merloni A., Rees M., 2001, *MNRAS*, 324, 1147  
 Rees M., Mészáros P., 1994, *ApJ*, 430, L93  
 Sari R., Piran T., Narayan R., 1998, *ApJ*, 497, L17  
 Troja E. et al, 2007, *ApJ*, 665, 599  
 Uhm Z., Beloborodov A., 2007, *ApJ*, 665, L93  
 Watson D. et al, 2006, *ApJ*, 652, 1011  
 Willingale R. et al, 2007, *ApJ*, 662, 1093  
 Yost S. et al, 2007, *ApJ*, 657, 925  
 Zhang B. et al, 2006, *ApJ*, 642, 354